© The Authors. CC BY 4.0 Int. Licencee: SV-JME

Evaluation of Measurement Uncertainty in Creep-Based Determination of Viscoelastic Material Functions of Polypropylene

Urban Kotnik – Alen Oseli – Jože Kutin – Miroslav Halilovič – Lidija Slemenik Perše ✉
Faculty of Mechanical Engineering, University of Ljubljana, Slovenia
✉ lidija.slemenik.perse@fs.uni-lj.si

Abstract *Modern numerical models use time-dependent material parameters as input data to simulate the viscoelastic response of polymers. Reliable numerical predictions therefore depend on the accurate determination of these parameters. Understanding the measurement uncertainty associated with their identification is essential for assessing the expected range and reliability of the simulation results. Although creep-based uncertainty analyses have been reported for other materials, uncertainty evaluations for polymers that require the determination of multiple viscoelastic material functions remain scarce, with existing polymer studies primarily relying on relaxation tests. This study experimentally analyzes the viscoelastic behavior of polypropylene at 60 °C through tensile and shear creep tests based on extensional and rotational rheometry. The tensile, shear, and bulk compliance functions were determined together with their corresponding standard and expanded measurement uncertainties in accordance with the JCGM 100:2008 guideline. Type A uncertainties were found to dominate the overall uncertainty, with relative expanded uncertainties of approximately 3 percent for shear compliance and up to 25 percent for bulk compliance. The study identifies the main sources of uncertainty and proposes strategies for their reduction, including increasing the number of measurement repetitions and improving environmental control. Overall, a comprehensive uncertainty evaluation of the creep-based determination of viscoelastic material functions is presented, leading to more reliable input data for numerical simulations.*

Keywords *viscoelasticity, creep test, polypropylene, measurement uncertainty*

Highlights

- *Uncertainty analysis for creep-based determination of multiple viscoelastic functions of polymers was preformed.*
- *Measurement uncertainties of tensile, shear, and bulk compliance functions of polypropylene at 60 °C were quantified.*
- *Bulk compliance shows relative expanded uncertainty exceeding 20 %.*
- *Strategies for uncertainty reduction: increased repetitions, improved instrumentation, and environmental control.*

1 INTRODUCTION

Polymers are increasingly used in industry, due to their low density compared to conventional engineering materials and the excellent mechanical properties they can achieve when combined with various fillers [1]. Because of their wide use in the automotive, construction, and medical industries, reliable prediction of their mechanical behavior is becoming crucial for product design. Consequently, there is a growing need for models and numerical simulations that adequately capture the viscoelastic response of these materials. A wide range of models have been developed and reported in the literature to describe viscoelastic behavior. Classical models capture the linear viscoelastic response, such as the Findley power law [2], the representation of material functions by a Prony series [3], and the standard linear solid model [4]. Under larger loads, nonlinear viscoelasticity emerges, which is well described by Schapery's model [5] and its derivatives [6,7,8]. By employing homogenization methods [9,10,11] or extending existing viscoelastic models to account for anisotropy [12,13,14], it is also possible to describe the behavior of more complex polymer composites.

For the application of these models in numerical programs based on the finite element method, knowledge of the time-dependent mechanical properties of the material is essential. These are most often expressed in terms of relaxation functions: the bulk modulus $K(t)$ and the shear modulus $G(t)$ [15]. Obtaining $K(t)$ directly is impractical and is usually determined indirectly through the tensile modulus $E(t)$ and shear modulus $G(t)$. The functions are determined on the basis of relaxation tests, which require loading the specimen with a constant strain. This poses a major challenge for many modern rheometers [3]. In practice, creep tests are therefore often employed, where the specimen is subjected to constant stress while measuring the tensile compliance $D(t)$ and shear compliance $J(t)$. From these, the bulk compliance $B(t)$ can be mathematically determined, allowing for the reconstruction of $K(t)$ and $G(t)$.

Accurate characterization of these material functions is crucial for credible numerical simulations of the viscoelastic response of polymers. The influence of measurement uncertainty on different polymer properties has already been analyzed: its impact on the glass transition temperature [16,17], on the deformation of elastomers [18], and on the tensile strength of cellulose fiber-reinforced polypropylene [19]. Beyond polymer-specific studies, similar challenges in obtaining realistic confidence intervals have been reported in inverse identification based on full-field measurements, where classical Gaussian error assumptions were shown to significantly underestimate parameter uncertainty [20].

Uncertainty analyses of material properties obtained form creep tests have also been reported in literature. For compressive creep tests of concrete, Jin et al. [21] and Criel et al. [22] determined the uncertainty of creep compliance. Madsen and Bazant [23]

investigated the uncertainty associated with creep shrinkage in concrete while Keitel et al. [24] focused on the uncertainty of creep strain. For asphalt materials, Kassem et al. [25] used creep test data to determine the uncertainty of both the relaxation modulus and creep compliance. Hossain et al. [26] conducted creep tests on steel alloys to quantify the uncertainty associated with time to creep failure.

With a focus on polymers, Adamczak [27] performed stress relaxation tests on polymers fabricated using 3D printing technology and analyzed the uncertainty associated with the parameters of the relaxation curve described by a rheological solid model. Lu et al. [28] investigated the possibility of obtaining the bulk modulus from shear and extension relaxation moduli and demonstrated the exponentially increasing sensitivity of the bulk modulus to relative errors in the shear modulus as the Poisson's ratio approaches 0.5. Michaeli et al. [29] also conducted tensile stress relaxation tests, however, unlike in [28], only tensile tests were performed. Using a novel analytical protocol based on probability density functions, they studied the uncertainties of material functions obtained through this approach.

From the above review, it is evident that for polymers, where a complete time-dependent characterization of the material requires information on multiple time-dependent material functions, uncertainty analyses associated with the determination of these functions remain scarce. While authors in [28] addressed the uncertainty of shear and extension moduli and its propagation to the bulk modulus, similar to other studies focusing on polymers, the material functions were obtained from relaxation tests. Although creep and relaxation are related time-dependent phenomena, they differ fundamentally in both the applied loading conditions and the measured responses, as well as in the resulting material functions. Moreover, creep testing is becoming increasingly favored in polymer characterization, as maintaining a constant stress is generally less challenging and more robust than enforcing a constant strain. Consequently, a comprehensive creep-based uncertainty analysis of the extension, shear, and bulk compliance functions is still lacking, revealing a clear research gap.

The central objective of this article is therefore to present the measurement procedure and the evaluation of the measurement uncertainties of the functions $D(t)$, $J(t)$, and $B(t)$ for polypropylene in accordance with JCGM 100:2008 [30], as these directly affect the accuracy of numerical simulation results.

The following sections first introduce the theoretical background of creep tests, followed by the measurement procedure, results and discussion of the uncertainty analysis.

2 METHOD

2.1 Constitutive Equations of Viscoelasticity

In viscoelastic materials, such as polymers, the response to loading is time-dependent. The current stress in the material depends not only on the present strain but also on all past strains [31,32]. The constitutive relation between stress σ and strain ε is therefore expressed by a convolution integral:

$$\sigma(t) = \int_0^t E(t-u)\frac{d\varepsilon(u)}{du}du, \tag{1}$$

where u denotes the past time in the convolution integral, and E is the Young's modulus. To describe viscoelastic isotropic materials in three dimensions using the bulk modulus $K(t)$ and the shear modulus $G(t)$, Eq. (1) is extended to three dimensions [33]:

$$\sigma_{ij} = 3\int_0^t K(t-u)\frac{d\varepsilon_{ij}^{vol}(u)}{du}du + 2\int_0^t G(t-u)\frac{d\varepsilon_{ij}^{dev}(u)}{du}du, \tag{2a}$$

$$K(t) = \frac{E(t)G(t)}{9G(t)-3E(t)}, \tag{2b}$$

where ε_{ij}^{vol} represents the volumetric part of the strain tensor, and ε_{ij}^{dev} the deviatoric part. The bulk modulus $K(t)$ is most commonly determined from $E(t)$ and $G(t)$. Commercial finite element analysis programs (e.g., Abaqus, Ansys) require input data in the form of $K(t)$ and $G(t)$ in order to predict the viscoelastic response.

2.2 Determination of Time-Dependent Material Functions

To avoid solving convolution integrals when determining time-dependent moduli, relaxation tests and creep tests are often employed. Within our measurement system, which will be described in more detail in Section 3.2, we cannot ensure constant strain, but we can impose constant stress. Due to this limitation, time-dependent functions will be determined using creep tests, in which the specimen is suddenly loaded with a constant stress σ_0 and the time evolution of strain $\varepsilon(t)$ is monitored. The tensile compliance $D(t)$ is in this case calculated as:

$$D(t) = \frac{\varepsilon(t)}{\sigma_0} = \frac{d^2\pi\Delta L(t)}{4FL}, \tag{3}$$

where F is the constant force applied to a cylindrical specimen of diameter d, L denotes the initial length, and $\Delta L(t)$ the change in specimen length. If the specimen is loaded with a constant shear stress τ_0 and the time evolution of shear strain $\gamma(t)$ is monitored, the shear compliance $J(t)$ can be determined:

$$J(t) = \frac{\gamma(t)}{\tau_0} = \frac{d^4\pi\varphi_t(t)}{32M_tL}. \tag{4}$$

τ_0 results from the application of a constant torsional moment M_t, while the shear strain is calculated from the twist angle $\varphi_t(t)$. It is important to emphasize that the magnitudes of the stresses σ_0, τ_0 are sufficiently small to ensure that the material response remains within the linear viscoelastic region (LVR), where the time-dependent response is a consequence of the time dependence of the material and not the magnitude of the load [15]. All quantities that need to be measured in order to determine $D(t)$ and $J(t)$ are shown in Fig. 1. Once the quantities $J(t)$ and $D(t)$ are obtained, a transformation into the Laplace domain is performed, where in Eq. (2b) we consider $B(s)=1/K(s)$, $J(s)=1/G(s)$, $D(s)=1/E(s)$, and determine the bulk compliance $B(s)$:

$$B(s) = 9D(s) - 3J(s). \tag{5}$$

Based on the compliance functions, the functions $K(t)$ and $G(t)$ required for numerical simulations are calculated. The uncertainty with which the compliance $J(t)$ is determined is thus directly related to the uncertainty of the function $G(t)$ ($u(J(t)) \propto u(G(t))$). The same holds for the bulk functions ($u(B(t)) \propto u(K(t))$). In Equation (5), we will neglect the need for transformation into the Laplace domain:

$$B(t) = 9D(t) - 3J(t), \tag{6}$$

which will later allow us to also estimate the uncertainty for the function $B(t)$.

3 EXPERIMENTAL

3.1 Material and Specimen Preparation

In this study, we examine polypropylene, supplied in granule form by the company Inno-Comp, Hungary. Injection molding was carried out after drying of the granules for 4 hours at 100 °C and then mixing for 5 minutes at 210 °C with a screw speed of 50 rpm. During molding, the barrel temperature was 210 °C and the mold

temperature was 90 °C. Injection lasted 10 s at a pressure of 5 MPa, followed by a holding phase at 10 MPa. The molded part is shown in Fig. 2a, from which two cylindrical specimens were cut. During the injection molding process, the rapid cooling of the material freezes the motion of polymer chains, causing residual thermomechanical stresses, which in turn lead to larger deviations between individual measurements [34]. Through heat treatment, where the material is kept for an extended time at a constant temperature above the glass transition temperature T_g and then cooled very slowly, the molecules are given sufficient time to rearrange into the energetically most favorable configuration. The heat treatment process, used for the specimen, is illustrated in Fig. 2b.

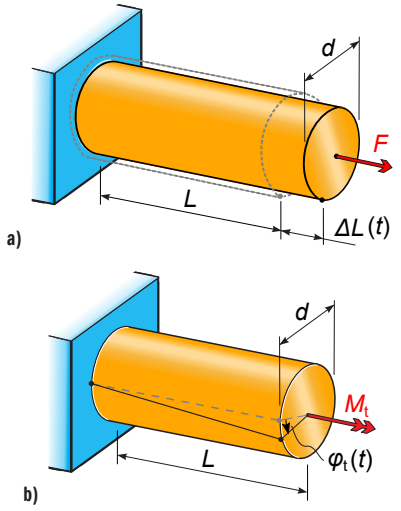

Fig. 1. Measured parameters in a creep test; a) tensile creep test, b) shear creep test

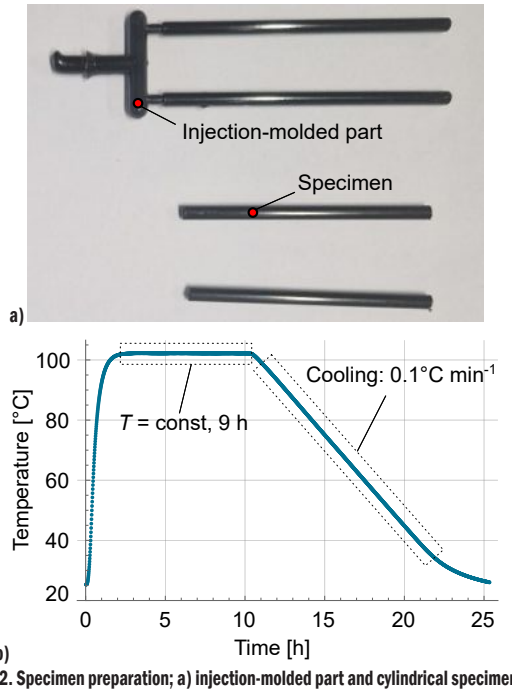

Fig. 2. Specimen preparation; a) injection-molded part and cylindrical specimen, and(b) heat treatment of the specimen

3.2 Measurement System and Experimental Procedure

Measurements of the functions $D(t)$ and $J(t)$ were carried out using a MCR702 rheometer (Modular Compact Rheometer, Anton Paar, Austria) [35] and the RheoCompass software. The experimental setup for creep testing is shown in Fig. 3.

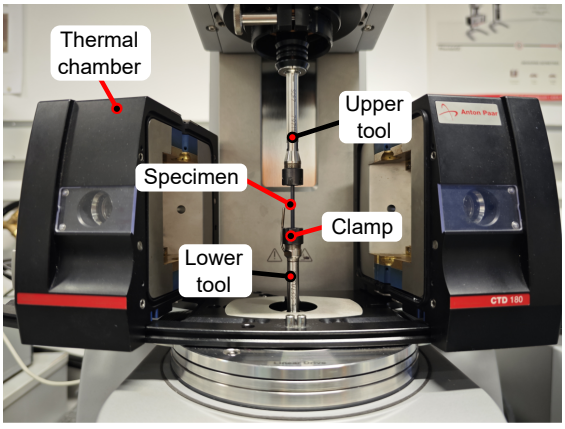

Fig. 3. Preparation of the creep measurement on the MCR702 rheometer

The specimen diameter d was measured with a 412821-150 digital caliper (Holex, München, Germany). The specimen was then clamped between the upper and lower tool, with both clamps tightened using a torque wrench set to 0.4 Nm. The effective clamping length L was determined by the encoder of the motor responsible for lifting the measuring head. Finally, the specimen was enclosed in a thermal chamber. Three repetitions of the tensile creep test and three repetitions of the shear creep test were performed. In the tensile test, only the linear actuator connected to the lower tool was active, while the rotational actuator, connected to the upper tool, remained stationary. In the shear test, only the rotational actuator was active. All measurements were conducted at a temperature of 60 °C. The experimental procedure is illustrated in Fig. 4.

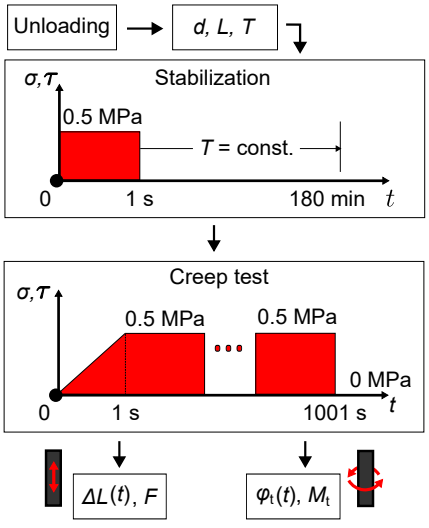

Fig. 4. Creep experiment procedure and parameters.

Using the RheoCompass software, the system was first unloaded, after which the measured geometric parameters d and L and the temperature T were entered. This was followed by a stabilization phase, during which the specimen was suddenly loaded for one second with a stress of 0.5 MPa to ensure proper alignment and good contact between the cylindrical specimen and the clamps. Before starting the measurement, a waiting period of 180 min was applied to eliminate the influence of the pre-applied stress on the results and to allow the specimen to reach the uniform target temperature. The creep test was performed in two phases. In the first phase, the stress was linearly increased within one second to 0.5 MPa. In the tensile test, the normal stress σ_0 was controlled, whereas in the shear test the shear stress τ_0 was controlled. Although, in theory, the stress

step should be infinitely short, this is avoided in practice to prevent inertial effects and possible vibrations. In the second phase, the specimen was loaded with a constant stress for 1000 s. In the tensile test, the program recorded the force F required to establish σ_0 and the specimen elongation $\Delta L(t)$. In the shear test, the torsional moment M_t required to establish τ_0 was measured, as well as the change in twist angle $\varphi_t(t)$ as a result of shear creep.

3.3 Evaluation of Measurement Uncertainty

With heat treatment, we avoided potential uncertainties arising from residual compressive stresses. The experimental procedure described in Section 3.2, directly contributes to reducing uncertainties related to clamping and load application. In addition, by applying small stresses to the specimen, we ensured that the material remained in the LVR so the response depended only on time and not on the magnitude of the load. During all tests, the thermal chamber maintained a constant temperature of approximately T=60 °C with a stability of 0.02 °C. Consequently, the sources of uncertainty were limited to the following dependencies: $D(t)=D(L,d,F,\Delta L(t))$ and $J(t)=J(L,d,M_t,\varphi_t(t))$. Next, type A and type B uncertainties were calculated. Type A uncertainty is evaluated from the statistical analysis of repeated observations, while type B uncertainty is estimated by other means, such as calibration certificates or technical specifications of measurement instruments.

Table 1 presents the type B standard uncertainties of the rheometer, for which uncertainties were determined from both the calibration (u_B^{cal}) and the resolution ($u_B^{res} = res/\left(2\sqrt{3}\right)$), while for the digital caliper, the uncertainty was estimated solely based on its resolution $u_B^{res}(d) = 2.9 \cdot 10^{-3}$.

Table 1. Type B standard uncertainties for rheometer Anton Paar MCR702e

x	$u_B^{cal}(x)$	$res(x)$	$u_B^{res}(x)$
L [mm]	$4.6 \cdot 10^{-2}$	$1.0 \cdot 10^{-3}$	$2.9 \cdot 10^{-4}$
ΔL [mm]	$2.0 \cdot 10^{-5}$	$1.0 \cdot 10^{-9}$	$2.9 \cdot 10^{-10}$
F [N]	$5.0 \cdot 10^{-3}$	$1.0 \cdot 10^{-3}$	$2.9 \cdot 10^{-4}$
M_t [Nmm]	$3.7 \cdot 10^{-3}$	$1.0 \cdot 10^{-6}$	$2.9 \cdot 10^{-7}$
φ_t [rad]	$4.0 \cdot 10^{-5}$	$1.0 \cdot 10^{-9}$	$2.9 \cdot 10^{-10}$

According to the JCGM100:2008 standard [30], we calculated the combined standard measurement uncertainties, where $u(B(t))$ depends exclusively on $u(D(t))$ and $u(J(t))$.

$$u(B(t)) = \sqrt{\left(9u(D(t))\right)^2 + \left(-3u(J(t))\right)^2} \tag{7}$$

Using Student's t-distribution, we determined the effective degrees of freedom for a 95.45 % level of confidence, obtained the coverage factor k, and calculated the expanded measurement uncertainties $U=k \cdot u$. The equations for determining the combined standard uncertainties $u(D(t))$, $u(J(t))$ and $u(B(t))$ and the expanded measurement uncertainties $u(D(t))$, $u(J(t))$ and $u(B(t))$ are provided in the Appendix.

4 RESULTS AND DISCUSSION

The measured data from all test repetitions used in the uncertainty analysis are presented below. Table 2 presents the results of measurements of the time-independent quantities from the tensile and shear creep tests. Figure 5a shows the change in specimen length as a result of constant normal loading, while Fig. 5b illustrates the change in twist angle due to constant torsional moment. The measurement precision differs between tensile and shear tests. From the graphs in Fig. 5, it is evident that the curves for $\varphi_t(t)$ are smoother compared to the data for $\Delta L(t)$. Despite the higher resolution of the encoder used to measure $\Delta L(t)$, these measurements are more strongly affected by noise, which contributes to increased measurement uncertainty. The shear test exhibits greater variability among individual specimens, further increasing the uncertainty of the results.

Table 2. Results of the tensile and shear creep tests – time-independent quantities

	Tensile creep test (T = 60 °C)			Shear creep test (T = 60 °C)		
	d [mm]	L [mm]	F [N]	d [mm]	L [mm]	F [N]
Specimen 1	2.97	30.87	2.57	2.96	30.90	3.4
Specimen 2	2.97	30.87	2.56	2.97	30.92	3.45
Specimen 3	2.97	30.78	2.56	2.97	30.87	3.46

Table 3. Contributions of individual uncertainty sources relative to the combined standard measurement uncertainty

x	$\frac{x^2}{u(D(t))^2} \cdot 100$ [%]	x	$\frac{x^2}{u(J(t))^2} \cdot 100$ [%]
$u(D(t))$	100.00	$u(J(t))$	100.00
$u_A(D(t))$	**65.66**	$u_A(J(t))$	**77.79**
$u_B(D(t))$	**34.34**	$u_B(J(t))$	**22.21**
$c_1 \cdot u_B^{res}(d)$	**14.58**	$c_5 \cdot u_B^{res}(d)$	**16.45**
$c_2 \cdot u_B^{cal}(L)$	8.50	$c_6 \cdot u_B^{cal}(L)$	2.41
$c_3 \cdot u_B^{cal}(F)$	8.06	$c_7 \cdot u_B^{cal}(M_t)$	2.26
$c_4 \cdot u_B^{cal}(\Delta L(t))$	3.18	$c_8 \cdot u_B^{cal}(\varphi_t(t))$	1.10

Some of the observed variability in time-dependent deformation for both tensile and shear tests may be attributed to differences in morphological structure, particularly the degree of crystallinity, as well as to variations in the fraction of free volume, which governs chain mobility in viscoelastic solids. Additional contributions may arise from differences in molecular chain entanglement, molecular weight, and the degree of structural inhomogeneity between samples.

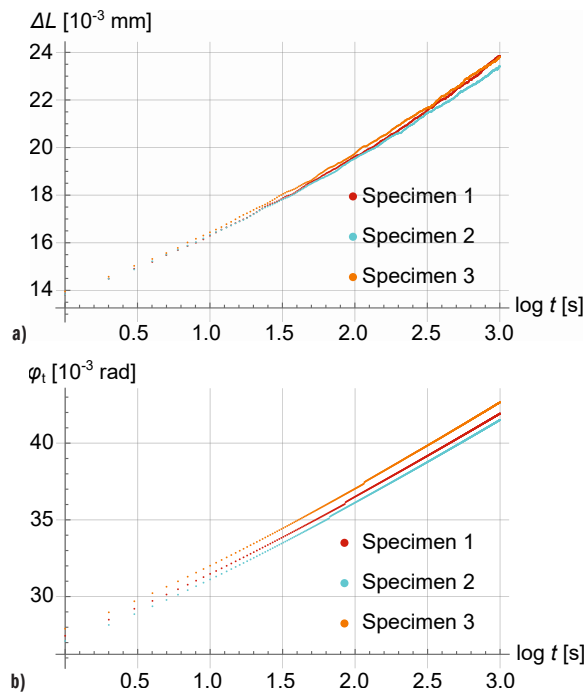

Fig. 5. Results of the creep test – time-dependent quantities; a) $\Delta L(t)$ measured in the tensile test, and b) $\varphi_t(t)$ measured in the shear test

The coverage factors determined from Student's distribution are shown in Fig. 6.

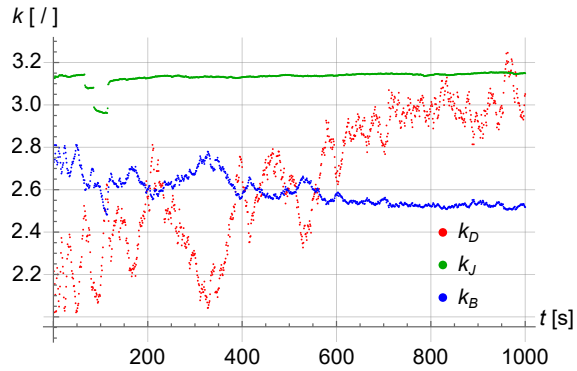

Fig. 6. Coverage factors for a 95.45 % level of confidence

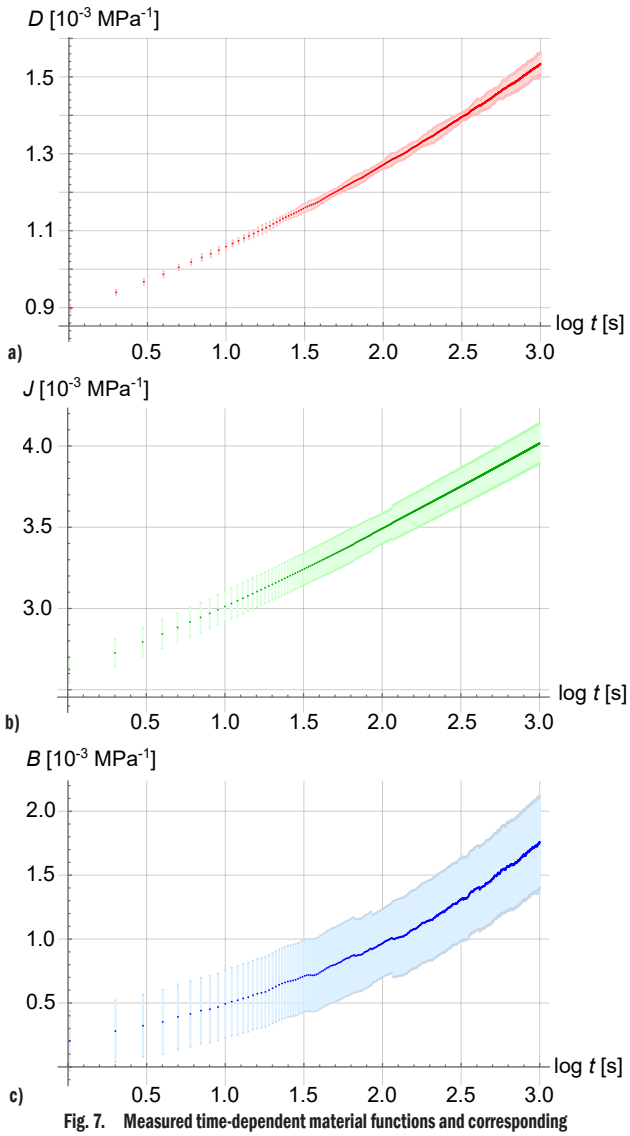

Fig. 7. Measured time-dependent material functions and corresponding expanded measurement uncertainties: a) $D(t)$, b) $J(t)$, and c) $B(t)$

The obtained coverage factors were higher than the value of $k=2$, which is characteristic of a Gaussian distribution for the same level of confidence. The increase in the value of k_D over time results from the growing experimental standard deviation of the measured change in specimen length, relative to its value $s(\Delta L(t))/\Delta L(t)$, while this ratio remains more constant for $\varphi_t(t)$. Local fluctuations in k_D originate from noise in the measurement of $\Delta L(t)$, while the discontinuity in k_J stems from discontinuities in the data $\varphi_t(t)$. This occurs in all three specimens and appears between 50 and 150 seconds from the start of the measurement shown in Fig. 5b, indicating a repeatable, systematic error of the measuring device.

The expanded measurement uncertainties revealed significant differences in the accuracy of the tensile, shear, and bulk compliance functions. Based on the mean values $\bar{D}(t)$, $\bar{J}(t)$, and $\bar{B}(t)$, the corresponding expanded measurement uncertainties $U(D(t))$, $U(J(t))$, and $U(B(t))$, are calculated and are shown in Fig. 7.

The estimated values are shown in Fig. 7 in darker color, while lighter shades represent the expanded uncertainties. The graphs show that the relative expanded uncertainty $U_r = U(x)/x$ is larger for $J(t)$ than for $D(t)$. In the case shown in Fig. 7c, this ratio increases even further.

To assess the quality of the measurements, we calculated the combined standard relative uncertainty u_r, the values of the coverage factors k, and the relative expanded uncertainty U_r. Since all quantities considered represent time series, they were averaged over the entire time domain, and the results are presented in Table 4.

Table 4. Time-averaged measurement uncertainties and level of confidence coefficients for the analyzed time range

	$\langle u_r \rangle$ [%]	$\langle k \rangle$ [1]	$\langle U_r \rangle$ [%]
$D(t)$	0.50	2.64	**1.34**
$J(t)$	0.97	3.13	**3.03**
$B(t)$	9.55	2.59	**24.87**

Although the relative combined standard uncertainties of $D(t)$ and $J(t)$ do not exceed 1 %, the relative standard uncertainty of $B(t)$ reaches almost 10 %, which is consistent with the sensitivity coefficients given in Eq. (7). The expanded measurement uncertainties are relatively high. In the case of $B(t)$, the expanded uncertainty reaches nearly 25 %. The high values of the coverage factors k also contribute to the increased expanded uncertainties. A reduction in the type A uncertainty could be achieved by increasing the number of measurement repetitions, which would simultaneously reduce the coverage factor k. Using a micrometer instead of a caliper would further decrease the uncertainty associated with the measurements of specimen dimensions. In addition, environmental factors that were not controlled, such as air humidity, may also contribute to the uncertainty of the results. Polymers are sensitive to moisture, as their mechanical properties deteriorate significantly with increasing humidity. If the measurements were not performed under the same relative humidity conditions, this could introduce a systematic error in the results.

5 CONCLUSIONS

The objective of this work was to evaluate the measurement uncertainty associated with creep-based material functions used in numerical modeling of viscoelastic response. In this study, the viscoelastic behavior of polypropylene at 60 °C was experimentally analyzed, with a focus on determining the time-dependent compliance functions: tensile $D(t)$, shear $J(t)$, and bulk $B(t)$ compliances. Based on extensional and rotational rheometry, the material functions were obtained from creep experiments, with each tensile and shear test repeated three times. The relative expanded uncertainty $U_r(J(t))$ was found to be 3.03 %, while $U_r(B(t))$ reached 24.87 %.

The experimentally measured functions $J(t)$ and $D(t)$, together with the derived bulk compliance $B(t)$, can be transformed into relaxation moduli commonly used in commercial finite element solvers, enabling direct implementation of the present results and their associated uncertainty bounds in numerical simulations. This

facilitates a more informed and critical use of experimental material data in engineering analyses. To improve the reliability of the results, type A measurement uncertainty can be reduced by increasing the number of repeated measurements and improving environmental control. Nevertheless, even when $J(t)$ and $D(t)$ are measured with higher accuracy, uncertainty propagation leads to values of $U(B(t))$ that are approximately one order of magnitude larger, emphasizing the importance of uncertainty analysis in viscoelastic modeling.

References

[1] Gusev, A.A. . Finite *Element Estimates of Viscoelastic Stiffness of Short Glass Fiber Reinforced Composites*. *Compos Struct* 171 53–62 (2017) **DOI:10.1016/j.compstruct.2017.03.021**.

[2] Findley, W.N. *Mechanism and Mechanics of Creep of Plastics and Stress Relaxation and Combined Stress Creep of Plastics*. Division of Engineering, Brown University (1960).

[3] Park, S.W., Schapery, R.A. Methods of Interconversion between Linear Viscoelastic Material Functions. Part I-a Numerical Method Based on Prony Series. *Int J Solids Struct* 36 1653–1675 (1999) **DOI:10.1016/S0020-7683(98)00055-9**.

[4] Lin, C.-Y. Alternative form of standard linear solid model for characterizing stress relaxation and creep: Including a novel parameter for quantifying the ratio of fluids to solids of a viscoelastic solid. *Front Mater* 7 11 (2020) **DOI:10.3389/fmats.2020.00011**.

[5] Schapery, R.A. On the characterization of nonlinear viscoelastic materials. *Polym Eng Sci* 9 295–310 (1969) **DOI:10.1002/pen.760090410**.

[6] Henriksen, M. Nonlinear viscoelastic stress analysis—a finite element approach. *Comput Struct* 18 33–139 (1984) **DOI:10.1016/0045-7949(84)90088-9**.

[7] Lai, J., Bakker, A. 3-D schapery representation for non-linear viscoelasticity and finite element implementation. *Comput Mech* 18 182–191 (1996) **DOI:10.1007/BF00369936**.

[8] Haj-Ali, R., Muliana, A. Numerical finite element formulation of the schapery non-linear viscoelastic material model. *Int J Numer Methods Eng* 59 25–45 (2004). **DOI:10.1002/nme.861**.

[9] Sosa-Rey, F., Lingua, A., Piccirelli, N., Therriault, D., Lévesque, M. Thermo-viscoelastic multiscale homogenization of additively manufactured short fiber reinforced polymers from direct microstructure characterization. *Int J Solids and Struct* 281 112421 (2023) **DOI:10.1016/j.ijsolstr.2023.112421**.

[10] Wang, Z., Smith, D.E. Numerical analysis on viscoelastic creep responses of aligned short fiber reinforced composites. *Comp Struct* 229 111394 (2019) **DOI:10.1016/j.compstruct.2019.111394**.

[11] Cruz-González, O.L., Ramírez-Torres, A., Rodríguez-Ramos, R., Otero, J.A., Penta, R., Lebon, F. Effective behavior of long and short fiber-reinforced viscoelastic composites. *Appl Eng Sci* 6 100037 (2021) **DOI:10.1016/j.apples.2021.100037**.

[12] Amir i-Rad, A., Pastukhov, L.V., Govaert, L.E., Van Dommelen, J.A.W. (2019). An anisotropic viscoelastic-viscoplastic model for short-fiber composites. *Mech Mater* 137 103141 **DOI:10.1016/j.mechmat.2019.103141**.

[13] Fliegener, S., Hohe, J. An anisotropic creep model for continuously and discontinuously fiber reinforced thermoplastics. *Compos Sci Technol* 194 108168 (2020) **DOI:10.1016/j.compscitech.2020.108168**.

[14] Zobeiry, N., Malek, S., Vaziri, R., Poursartip, A. (2016). A differential approach to finite element modelling of isotropic and transversely isotropic viscoelastic materials. *Mech Mater* 97 76–91 **DOI:10.1016/j.mechmat.2016.02.013**.

[15] Endo, V.T., De Carvalho Pereira, J.C. (2017). Linear orthotropic viscoelasticity model for fiber reinforced thermoplastic material based on prony series. *Mech Time-Depend Mater* 21 199–221 **DOI:10.1007/s11043-016-9326-8**.

[16] Jha, A., Chandrasekaran, A., Kim, C., Ramprasad, R. Impact of dataset uncertainties on machine learning model predictions: the example of polymer glass transition temperatures. *Model Simul Mater Scie Eng* 27 024002 (2019) **DOI:10.1088/1361-651X/aaf8ca**.

[17] Alzate-Vargas, L., Fortunato, M.E., Haley, B., Li, C., Colina, C.M., Strachan, A. Uncertainties in the predictions of thermo-physical properties of thermoplastic polymers via molecular dynamics. *Model Simul Mater Scie Eng* 26 065007 (2018) **DOI:10.1088/1361-651X/aace68**.

[18] Miles, P., Hays, M., Smith, R., Oates, W. Bayesian uncertainty analysis of finite deformation viscoelasticity. *Mech Mater* 91 35-49 (2015) **DOI:10.1016/j.mechmat.2015.07.002**.

[19] Mokaloba, N., Batane, R. Evaluation of uncertainty of measurement for cellulosic fiber and isotactic polypropylene composites subjected to tensile testing. *Int J Eng Sci Technol* 7 70-79 (2015) **DOI:10.4314/ijest.v7i2.6**.

[20] Maček, A., Starman, B., Coppieters, S., Urevc, J., Halilovič, M. Confidence intervals of inversely identified material model parameters: A novel two-stage error propagation model based on stereo DIC system uncertainty. *Opt Lasers Eng* 174 107958 (2024) **DOI:10.1016/j.optlaseng.2023.107958**.

[21] Jin, S.-S., Cha, S.-L., Jung, H.-J. Improvement of concrete creep prediction with probabilistic forecasting method under model uncertainty. Const Build Mater 184 617-633 (2018) **DOI:10.1016/j.conbuildmat.2018.06.238**.

[22] Criel, P., Reybrouck, N., Caspeele, R., Matthys, S. Uncertainty quantification of creep in concrete by Taylor expansion. *Eng Struct* 153 334-341 (2017) **DOI:10.1016/j.engstruct.2017.10.004**.

[23] Madsen, H.O., Bažant, Z.P. Uncertainty analysis of creep and shrinkage effects in concrete structures. *ACI J* 80 116-127 (1983) **DOI:10.14359/10467**.

[24] Keitel, H., Dimmig-Osburg, A. Uncertainty and sensitivity analysis of creep models for uncorrelated and correlated input parameters. *Eng Struct* 32 3758-3767 (2010) **DOI:10.1016/j.engstruct.2010.08.020**.

[25] Kassem, H.A., Chehab, G.R., Najjar, S.S. Quantification of the inherent uncertainty in the relaxation modulus and creep compliance of asphalt mixes. Mech Time-Depend Mater 22 331-350 (2018) **DOI:10.1007/s11043-017-9359-7**.

[26] Hossain, M.A., Stewart, C.M. (2021). A probabilistic creep model incorporating test condition, initial damage, and material property uncertainty. *Int J Press Vessels Pip* 193 104446 **DOI:10.1016/j.ijpvp.2021.104446**.

[27] Adamczak, S., Bochnia, J. (2016). Estimating the approximation uncertainty for digital materials subjected to stress relaxation tests. *Metrol Meas Syst* 23 545-553 **DOI:10.1515/mms-2016-0048**.

[28] Lu, H., Zhang, X., Knauss, W.G. Uniaxial, shear, and Poisson relaxation and their conversion to bulk relaxation: studies on poly (methyl methacrylate). *Polym Compos* 18 211-222 (1997) **DOI:10.1002/pc.10275**.

[29] Michaeli, M., Shtark, A., Grosbein, H., Altus, E., Hilton, H.H. Uncertainty in characterizations of linear viscoelastic properties from 1-D tensile and dynamic experiments. *55th AIAA/ASME/ASCE/AHS/SC Structures,Structural Dynamics, and Materials Conference – SciTech Forum and Exposition* (2014).

[30] JCGM 100:2008. *Evaluation of measurement data — Guide to the expression of uncertainty in measurement (GUM)*. Joint Committee for Guides in Metrology, Sèvres Cedex (2008).

[31] Gutierrez-Lemini, D. *Engineering Viscoelasticity* 910 Springer New York (2014) **DOI:10.1007/978-1-4614-8139-3**.

[32] Ferry, J.D. *Viscoelastic Properties of Polymers*. John Wiley & Sons (1980).

[33] Aulova, A., Oseli, A., Bek, M., Prodan, T., Emri, I. Effect of pressure on mechanical properties of polymers. *Encyclopedia of Continuum Mechanics*. Springer, Berlin, Heidelberg 733-746 (2020) **DOI:10.1007/978-3-662-55771-6_270**.

[34] Oseli, A., Prodan, T., Susić, E., Slemenik Perše, L. (2020). The effect of short fiber orientation on long term shear behavior of 40% glass fiber reinforced polyphenylene sulfide. Polym Test 81 106262 **DOI:10.1016/j.polymertesting.2019.106262**.

[35] Anton Paar. Modular Compact Rheometer: MCR 702 MultiDrive, from *https://www.anton-paar.com/si-en/products/details/rheometer-mcr-702-multidrive/*, accessed on 20-03-2025.

Received: 2025-11-21, **revised:** 2026-02-04, **accepted:** 2026-02-12 *as Original Scientific Paper.*

Data availability *The data that support the findings of this study are available from the corresponding author upon reasonable request.*

Author contribution *U. Kotnik: Data Curation, Formal Analysis, Methodology, Visualization, Writing – Original Draft. A. Oseli: Investigation, Visualization. J. Kutin: Methodology, Writing – Review & Editing. M. Halilovič: Conceptualization, Writing – Review & Editing. L. Slemenik Perše: Supervision, Project Administration, Resources, Writing – Review & Editing.*

Appendix

The JCGM 100:2008 uncertainty evaluation consists of the following steps: (i) identification of significant influences on the accuracy of measurement results, (ii) evaluation of their standard measurement uncertainty (type A and type B methodology), (iii) determination of the combined standard measurement uncertainty, taking into account sensitivity coefficients and potential correlations between influences, (iv) determination of the expanded measurement uncertainty, taking into account an appropriate coverage factor. The expanded measurement uncertainty is usually determined for a confidence level of approximately 95 %, which in the case of a normal probability distribution means an increase in the combined standard measurement uncertainty by a coverage factor equal to 2. The calculation of the expanded measurement uncertainties using steps (ii-iv) is presented.

Type A uncertainty was determined based on Eqs. (3) and (4) and the experimental results. The arithmetic means of the quantities $J(t)$ and $D(t)$ were calculated:

$$\bar{D}(t)=\sum_{i=1}^{3}D_i(t)=\sum_{i=1}^{3}\frac{d_i^2\pi\Delta L_i(t)}{4F_iL_i}, \tag{8a}$$

$$\bar{J}(t)=\sum_{i=1}^{3}J_i(t)=\sum_{i=1}^{3}\frac{d_i^4\pi\varphi_{t,i}(t)}{32M_{t,i}L_i}, \tag{8b}$$

this was followed by the determination of the experimental standard deviation s:

$$s(D(t))=\sqrt{\frac{1}{3-1}\sum_{i=1}^{3}\left(D_i(t)-\bar{D}(t)\right)^2}, \tag{9a}$$

$$s(J(t))=\sqrt{\frac{1}{3-1}\sum_{i=1}^{3}\left(J_i(t)-\bar{J}(t)\right)^2}, \tag{9b}$$

and the determination of the type A standard measurement uncertainty:

$$u_A(D(t))=\frac{s(D(t))}{\sqrt{3}}, \tag{10a}$$

$$u_A(J(t))=\frac{s(J(t))}{\sqrt{3}}. \tag{10b}$$

The sensitivity coefficients were determined, and the combined standard measurement uncertainty for the tensile compliance $u_B(D(t))$ was calculated under the assumption of uncorrelated contributions:

$$u_B(D(t))=\frac{1}{3}\sum_{i=1}^{3}\sqrt{R_i^2}, \tag{11a}$$

$$R_i^2=\left(\left(\frac{\partial D(t)}{\partial d}\right)_i u_B^{res}(d)\right)^2+\left(\left(\frac{\partial D(t)}{\partial L}\right)_i u_B^{cal}(L)\right)^2+\left(\left(\frac{\partial D(t)}{\partial F}\right)_i u_B^{res}(F)\right)^2+\left(\left(\frac{\partial D(t)}{\partial F}\right)_i u_B^{cal}(F)\right)^2+\left(\left(\frac{\partial D(t)}{\partial \Delta L(t)}\right)_i u_B^{cal}(\Delta L(t))\right)^2, \tag{11b}$$

$$\left(\frac{\partial D(t)}{\partial d}\right)_i=\frac{d_i\pi\Delta L_i(t)}{2L_iF_i}, \tag{11c}$$

$$\left(\frac{\partial D(t)}{\partial L}\right)_i=-\frac{d_i^2\pi\Delta L_i(t)}{4L_i^2F_i}, \tag{11d}$$

$$\left(\frac{\partial D(t)}{\partial F}\right)_i=-\frac{d_i^2\pi\Delta L_i(t)}{4L_iF_i^2}, \tag{11e}$$

$$\left(\frac{\partial D(t)}{\partial \Delta L(t)}\right)_i=\frac{d_i^2\pi}{4L_iF_i}, \tag{11f}$$

and for the shear compliance $u_B(J(t))$:

$$u_B(J(t))=\frac{1}{3}\sum_{i=1}^{3}\sqrt{P_i^2}, \tag{12a}$$

$$P_i^2=\left(\left(\frac{\partial J(t)}{\partial d}\right)_i u_B^{res}(d)\right)^2+\left(\left(\frac{\partial J(t)}{\partial L}\right)_i u_B^{cal}(L)\right)^2+\left(\left(\frac{\partial J(t)}{\partial M_t}\right)_i u_B^{cal}(M_t)\right)^2+\left(\left(\frac{\partial J(t)}{\partial \varphi_t(t)}\right)_i u_B^{cal}(\varphi_t(t))\right)^2, \tag{12b}$$

$$\left(\frac{\partial J(t)}{\partial d}\right)_i=\frac{d_i^3\pi\varphi_{t,i}(t)}{8L_iM_{t,i}}, \tag{12c}$$

$$\left(\frac{\partial J(t)}{\partial L}\right)_i=-\frac{d_i^4\pi\varphi_{t,i}(t)}{32L_i^2M_{t,i}}, \tag{12d}$$

$$\left(\frac{\partial J(t)}{\partial M_t}\right)_i=-\frac{d_i^4\pi\varphi_{t,i}(t)}{32L_iM_{t,i}^2}, \tag{12e}$$

$$\left(\frac{\partial J(t)}{\partial \varphi_t(t)}\right)_i=\frac{d_i^4\pi}{32L_iM_{t,i}}. \tag{12f}$$

The contributions of type A and type B uncertainties were combined, and the combined standard measurement uncertainty was calculated:

$$u(D(t))=\sqrt{u_A(D(t))^2+u_B(D(t))^2}, \tag{13a}$$

$$u(J(t))=\sqrt{u_A(J(t))^2+u_B(J(t))^2}. \tag{13b}$$

For easier reading, the notations u_D and u_J are used instead of $u(D(t))$ and $u(J(t))$. The effective degrees of freedom υ_{eff} were determined:

$$\upsilon_{eff}^D=(3-1)\frac{u_D^4}{u_A(D(t))^4}, \tag{14a}$$

$$\upsilon_{eff}^J=(3-1)\frac{u_J^4}{u_A(J(t))^4}. \tag{14b}$$

Based on υ_{eff}, the coverage factors k_D and k_J for a 95.45 % level of confidence were determined from Student's t-distribution, and the expanded measurement uncertainty was calculated:

$$U\left(D(t)\right)=k_Du_D, \tag{15a}$$

$$U\left(J(t)\right)=k_Ju_J. \tag{15b}$$

Following the same procedure, and based on Eq. (6), the uncertainty $U(B(t))$ was also calculated:

$$\bar{B}(t)=9\bar{D}(t)-3\bar{J}(t), \tag{16a}$$

$$u(B(t))=\sqrt{(9u_D)^2+(-3u_J)^2}, \tag{16b}$$

$$\upsilon_{eff}^B=\frac{u(B(t))^4}{\frac{(9u_D)^4}{\upsilon_{eff}^D}+\frac{(-3u_J)^4}{\upsilon_{eff}^J}}, \tag{16c}$$

$$U(B(t))=k_Bu(B(t)). \tag{16d}$$

Vrednotenje merilne negotovosti pri določanju viskoelastičnih materialnih funkcij polipropilena na osnovi preizkusov lezenja

Povzetek *Sodobni numerični modeli uporabljajo časovno odvisne materialne parametre kot vhodne podatke za simulacijo viskoelastičnega odziva polimerov. Zanesljivost numeričnih napovedi je zato odvisna od točnosti določitve teh parametrov. Razumevanje merilne negotovosti, povezane z njihovo identifikacijo, je ključnega pomena za oceno pričakovanega razpona in zanesljivosti rezultatov simulacij. Čeprav so analize negotovosti na podlagi lezenja za druge materiale že znane, so vrednotenja negotovosti za polimere, ki zahtevajo določitev več viskoelastičnih materialnih funkcij, še vedno redka, obstoječe raziskave polimerov pa temeljijo predvsem na relaksacijskih preizkusih. Ta raziskava eksperimentalno analizira viskoelastično vedenje polipropilena pri 60 °C s pomočjo nateznih in strižnih preizkusov lezenja, ki temeljijo na natezni in rotacijski reometriji. Določene so bile natezna, strižna in stisljivostna podajnost ter pripadajoče standardne in razširjene merilne negotovosti v skladu s smernicami JCGM 100:2008. Rezultati kažejo, da negotovosti tipa A najbolj prispevajo k skupni standardni negotovosti, pri čemer so relativne razširjene negotovosti znašale približno 3 % za strižno podajnost in do 25 % za stisljivostno podajnost. Raziskava opredeljuje glavne vire negotovosti in predlaga strategije za njihovo zmanjšanje, vključno s povečanjem števila ponovitev meritev in izboljšanjem nadzora okoljskih pogojev. Predstavljeno je celovito vrednotenje negotovosti pri določanju viskoelastičnih materialnih funkcij na podlagi lezenja, kar zagotavlja zanesljivejše vhodne podatke za numerične simulacije.*

Ključne besede *viskoelastičnost, preizkus lezenja, polipropilen, merilna negotovost*